Indirect dark matter detection experiments

Mathias Garny

May 5, 2009

Gaisser,
Particle Physics and Cosmic Rays,
Cambridge Univ. Press (UK, 1990)

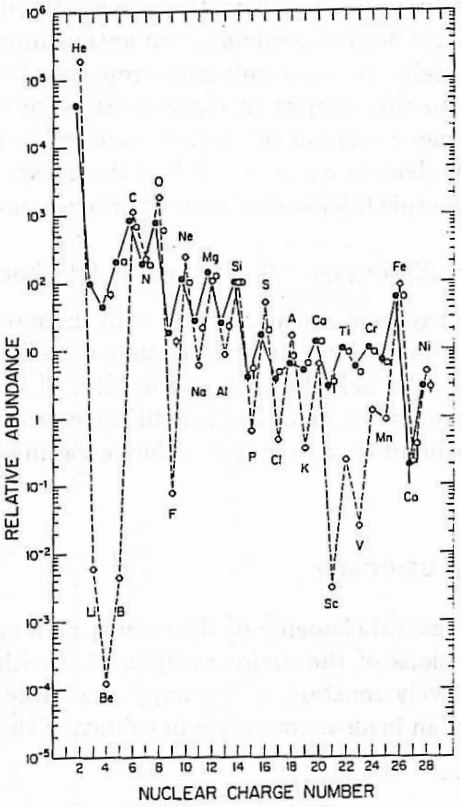

Figure 1.4: The cosmic ray elemental abundances (He-Ni) measured at Earth compared to the solar system abundances, all relative to silicon (from Simpson, 1983). (Reproduced with permission, from the *Annual Review of Nuclear and Particle Science,* Vol. 33, © 1983 by Annual Reviews Inc.)

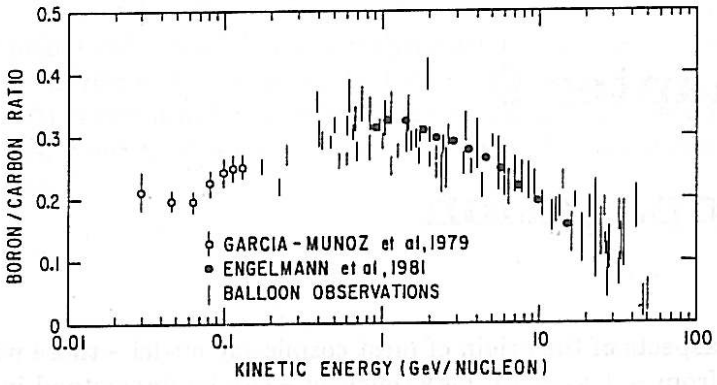

Figure 9.1: Summary of measurements of the ratio of boron to carbon from Ormes & Protheroe (1983). (Reprinted with permission from *The Astophysical Journal.*)

I.V. Moskalenko, A.W. Strong,

Production and propagation of cosmic ray positrons and electrons,

arXiv:astro-ph/9710124

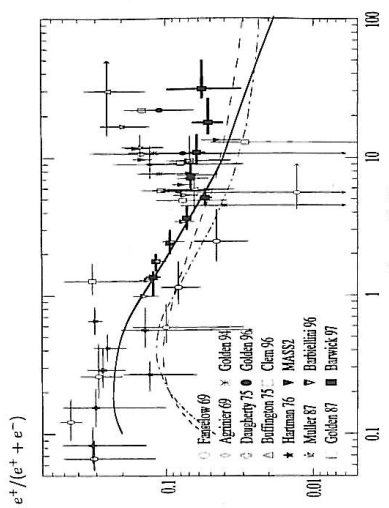

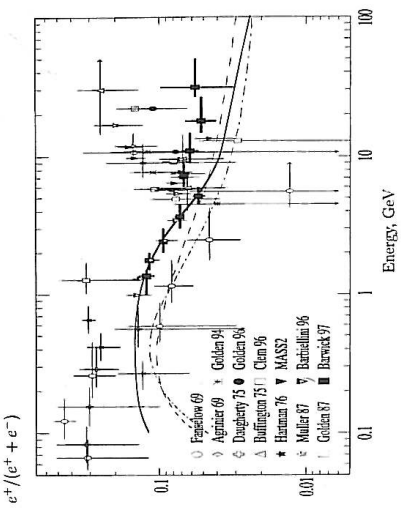

FIG. 7.—*Top panel*: positron fraction for model with no reacceleration. The positron spectrum is divided by the electron spectrum computed in the propagation model. The data and other curves are the same as in Fig. 6. *Bottom panel*: same positron fraction for model with reacceleration.

701

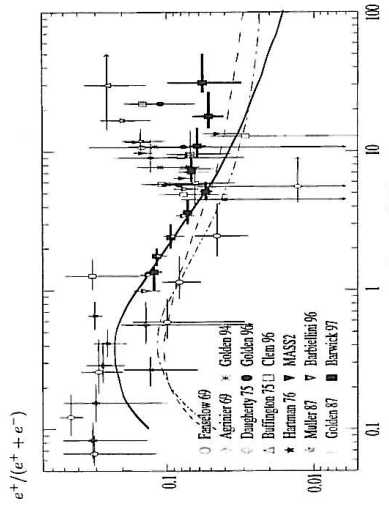

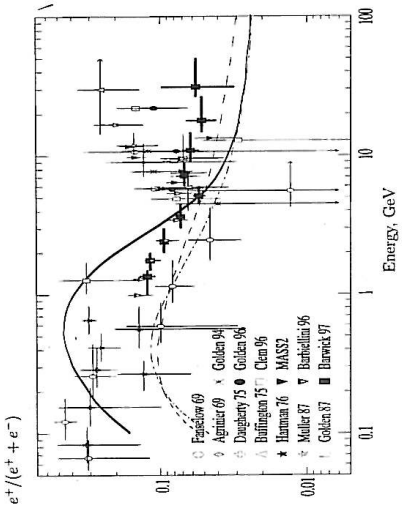

FIG. 6.—*Top panel*: positron fraction for model with no reacceleration. The positron spectrum is divided by the electron spectrum used by Protheroe (1982). *Dot-dashed line*: positron fraction from Protheroe (1982) leaky box (*dash-dotted*), diffusion (*dashed*). The collection of the experimental data is taken from Barwick et al. (1997). *Bottom panel*: same positron fraction for model with reacceleration.

700

Antiproton/Proton ratio, *PAMELA collaboration*, arXiv:0810.4994

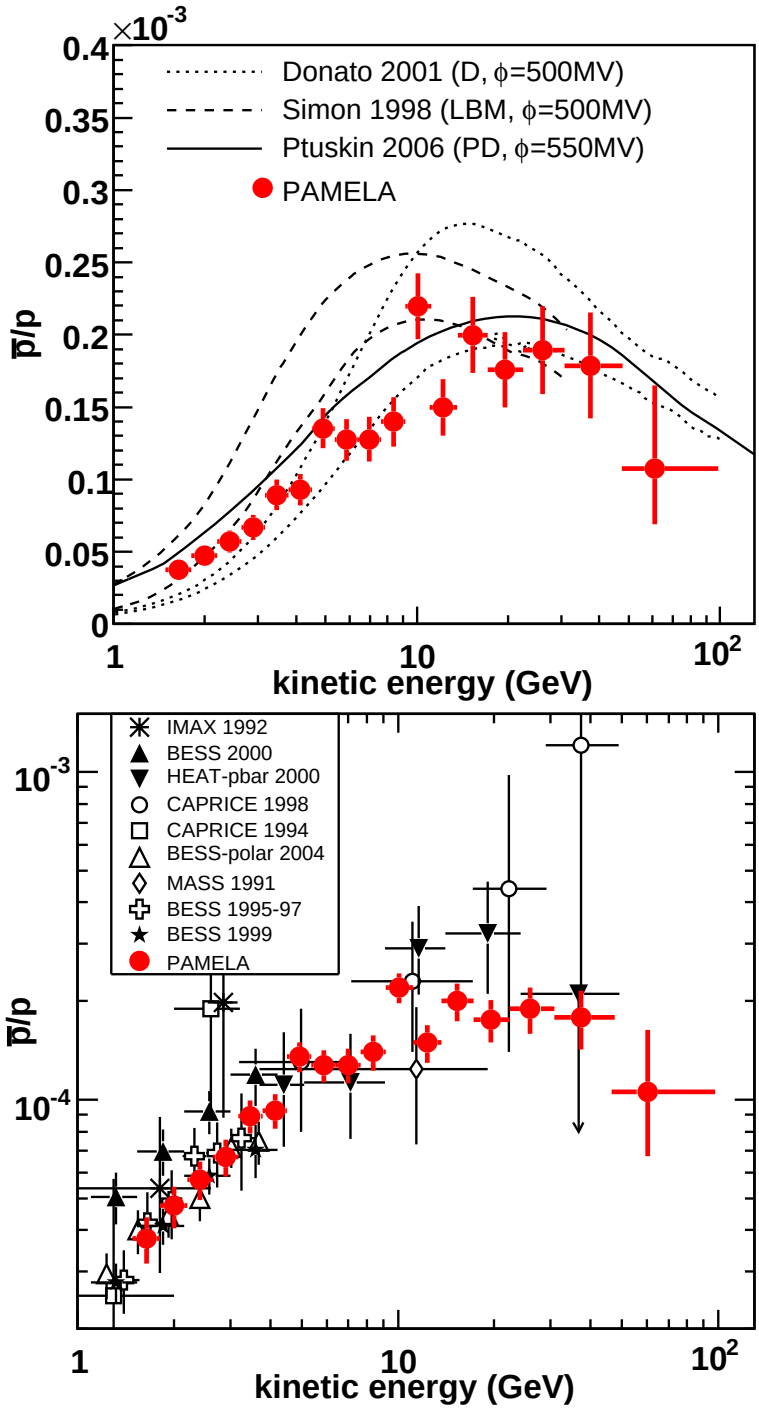

Positron fraction, *PAMELA collaboration*, arXiv:0810.4995

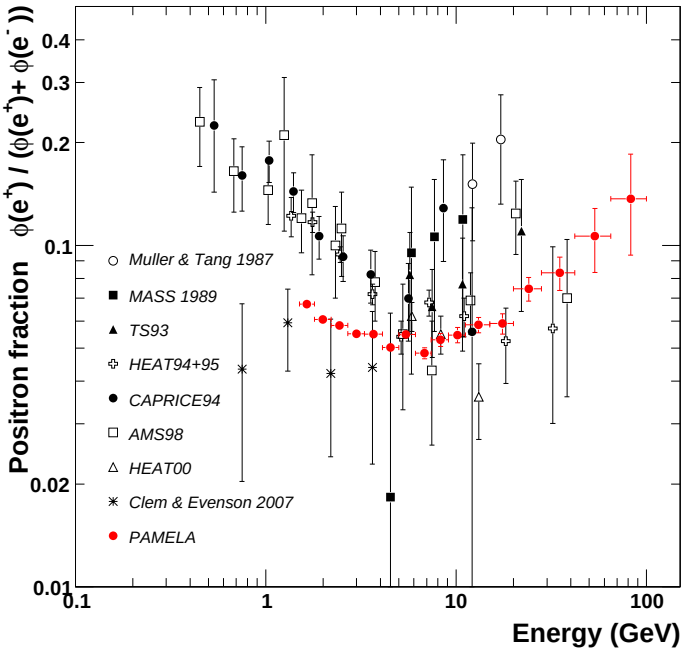

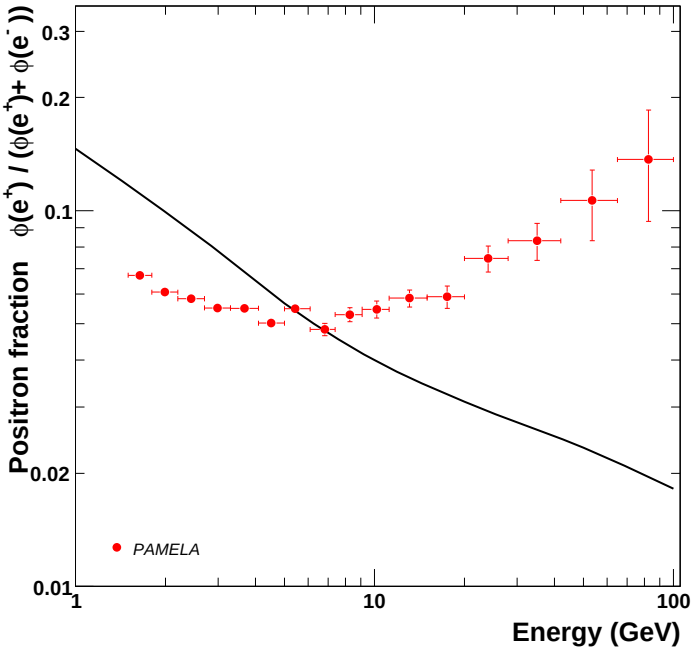

Solar modulation, *Grieder*, Cosmic Rays At Earth, Elsevier Science 2001

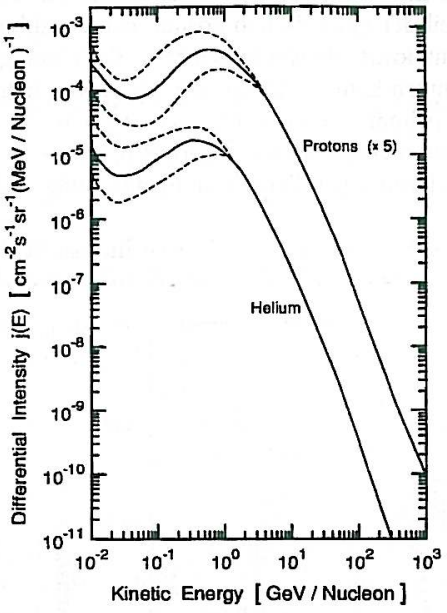

Abbildung 2.7:
Typisches differentielles Energiespektrum für Protonen und Heliumkerne der primären kosmischen Strahlung. Modulationseffekte sind durch die gestrichelten (Obere = Solmin, Untere = Solmax) und Mittelwerte durch durchgezogene Linien dargestellt. Das Protonenspektrum wurde mit einem Faktor fünf multipliziert, um graphischen Überlapp zu vermeiden [18].

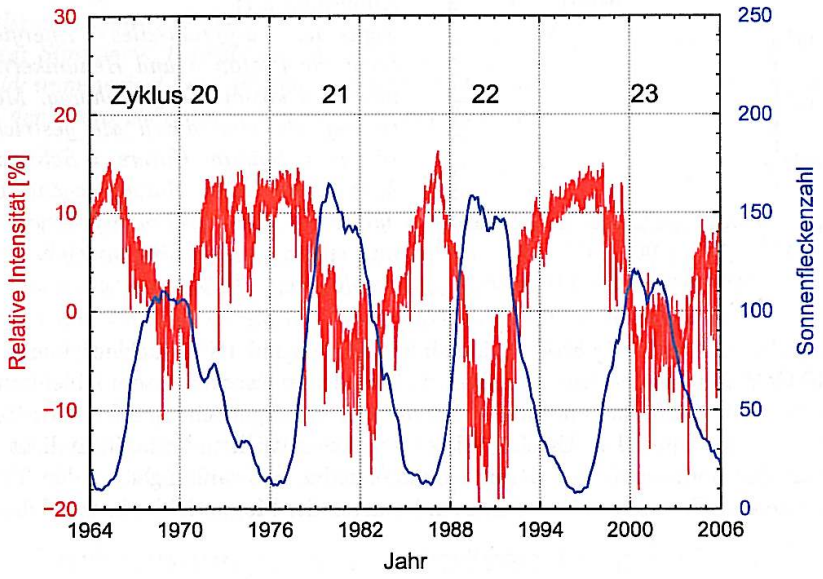

Abbildung 2.8: *Mittlere Sonnenfleckenanzahl (Blau)* [60] *und relative Intensität der kosmischen Strahlung auf der Erde (rot; normiert auf das Jahr 1960) als Funktion der Zeit; gemessen mit dem Climax-Neutronenmonitor, Colorado* [44].

[taken from C. Pioch, Diploma Thesis (TUM), 2008]

BESS,

arXiv:astro-ph/0109007

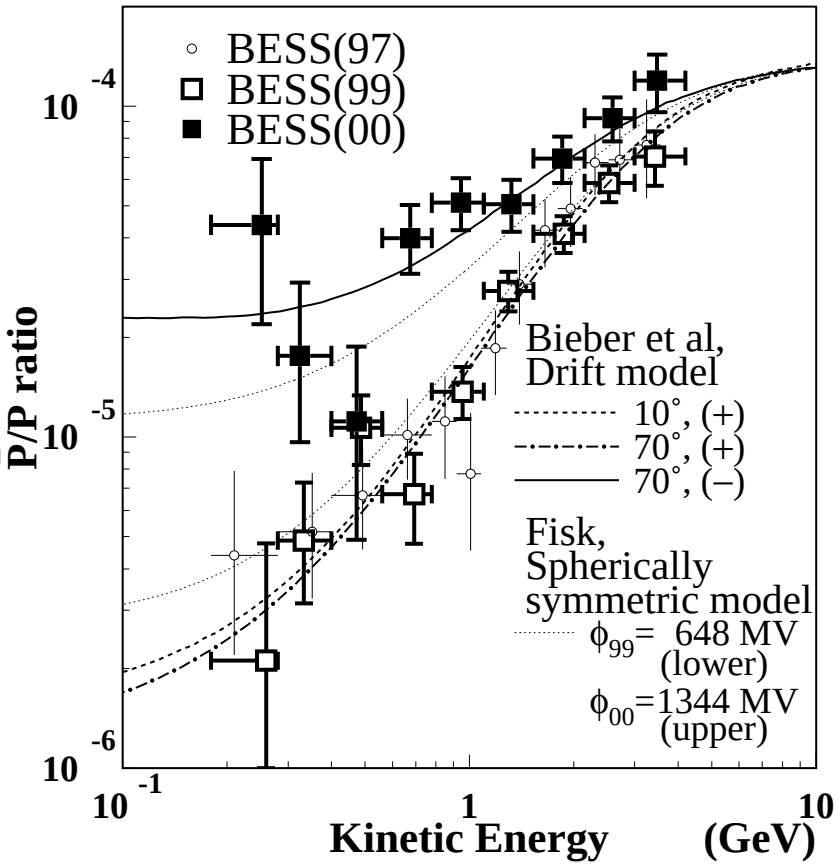

The $\bar{p}/p$ flux ratios measured by BESS in 1999 and 2000 with the previous data in 1997. The curves are calculations of the ratio at various solar activity

ATIC,
Nature 456:362-365,2008

Figure 2 | ATIC-1 and ATIC-2 spectra at balloon altitude, showing good agreement with each other. The measured primary electron flux (scaled by E^3) at flight altitude is shown for ATIC-1 (open squares) and ATIC-2 (filled circles). The errors are one standard deviation. Both balloon flights were from McMurdo, Antarctica, and circumnavigated that continent. ATIC-1 was a test flight in 2000–01 and the usable data correspond to an exposure of 0.61 m^2 sr days. ATIC-2 was a science flight in 2002–03 with an exposure of 2.47 m^2 sr days. To eliminate edge effects, we restrict the incident zenith angle to be less than ~37 ($\cos\theta \geq 0.8$), use only the central 80% of the SiM and eliminate events in the outer crystals in each BGO layer. Within these limits, the electron detection efficiency above 60 GeV is 84% essentially independent of energy. The effective acceptance was determined as a function of particle energy considering the trigger efficiency, trajectory reconstruction efficiency and the geometrical restrictions. The effective acceptance of the instrument increases from 0.075 m^2 sr at 20 GeV to 0.15 m^2 sr for $E > 60$ GeV. Above 100 GeV, a total of 1,724 electron events were observed, with the highest energy event at 2.3 TeV. The total background is also shown in the figure as the open triangles and is a combination of unresolved protons, unidentified γ-rays and atmospheric secondary electrons produced in the material (~4.5 g cm^{-2}) above the instrument. ATIC becomes background limited for electrons only above several teraelectronvolts.

Figure 3 | ATIC results showing agreement with previous data at lower energy and with the imaging calorimeter PPB-BETS at higher energy. The electron differential energy spectrum measured by ATIC (scaled by E^3) at the top of the atmosphere (red filled circles) is compared with previous observations from the Alpha Magnetic Spectrometer AMS (green stars)[11], HEAT (open black triangles)[30], BETS (open blue circles)[32], PPB-BETS (blue crosses)[16] and emulsion chambers (black open diamonds)[1,8,9], with uncertainties of one standard deviation. The GALPROP code calculates a power-law spectral index of −3.2 in the low-energy region (solid curve)[11]. (The dashed curve is the solar modulated electron spectrum and shows that modulation is unimportant above ~20 GeV.) From several hundred to ~800 GeV, ATIC observes an 'enhancement' in the electron intensity over the GALPROP curve. Above 800 GeV, the ATIC data returns to the solid line. The PPB-BETS data also seem to indicate an enhancement and, as discussed in Supplementary Information section 3, within the uncertainties the emulsion chamber results are not in conflict with the ATIC data.

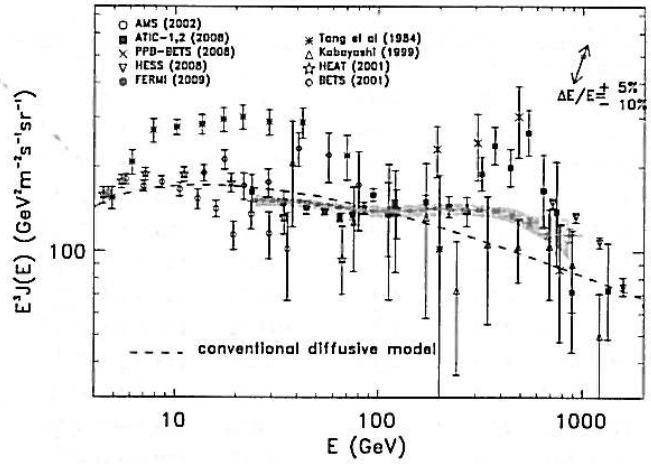

FIG. 3: (color) The Fermi LAT CR electron spectrum (red filled circles). Systematic errors are shown by the gray band. The two-headed arrow in the top-right corner of the figure gives size and direction of the rigid shift of the spectrum implied by a shift of $^{+5\%}_{-10\%}$ of the absolute energy, corresponding to the present estimate of the uncertainty of the LAT energy scale. Other high-energy measurements and a conventional diffusive model [1] are shown.

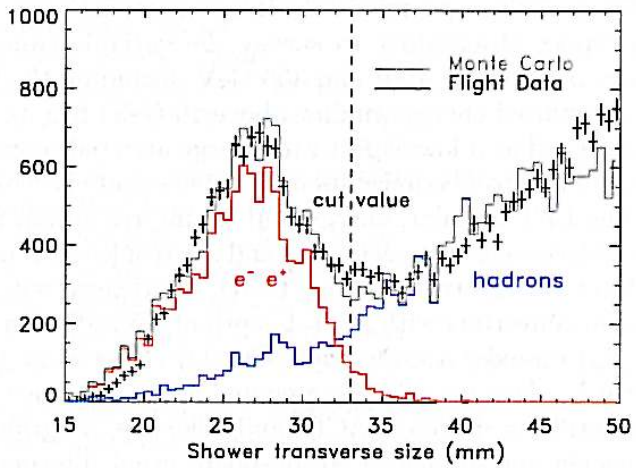

FIG. 2: (color online) Distribution of the transverse sizes of the showers (above 150 GeV) in the CAL at an intermediate stage of the selection, where a large contamination from protons is still visible. Flight data (black points) and MC (gray solid line) show very good agreement; the underlying distributions of electron and hadron samples are visible in the left (red) and the right (blue) peaks respectively.

HESS,

arXiv:0811.3894,arXiv:0905.0105

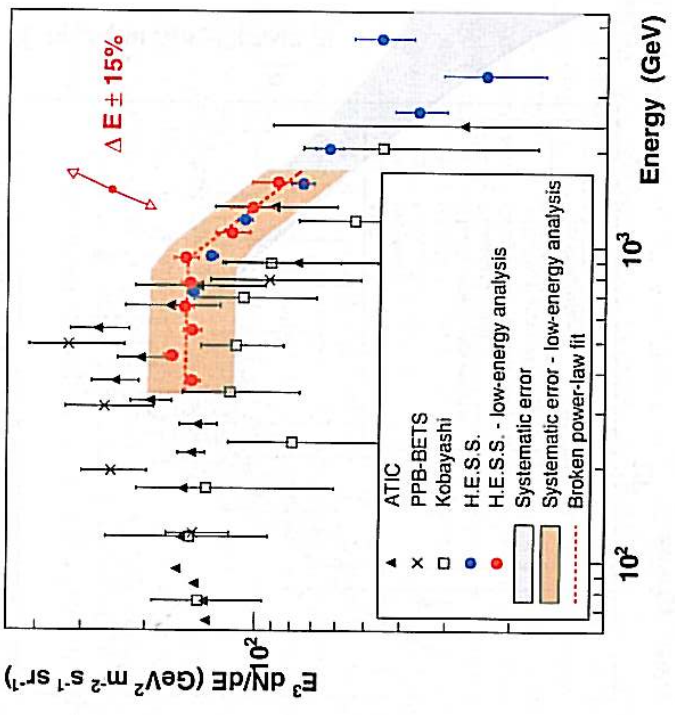

FIG. 2: The energy spectrum E^3 dN/dE of cosmic-ray electrons as measured by ATIC [4], PPB-BETS [12], emulsion chamber experiments [3] and H.E.S.S. Previous H.E.S.S. data [8] are shown as blue points, the result of the low-energy analysis presented here as red points. The shaded bands indicate the approximate systematic error arising from uncertainties in the modeling of hadronic interactions and in the atmospheric model in the two analyses. The double arrow indicates the effect of an energy scale shift of 15%, the approximate systematic uncertainty on the H.E.S.S. energy scale. The fit function is described in the text.

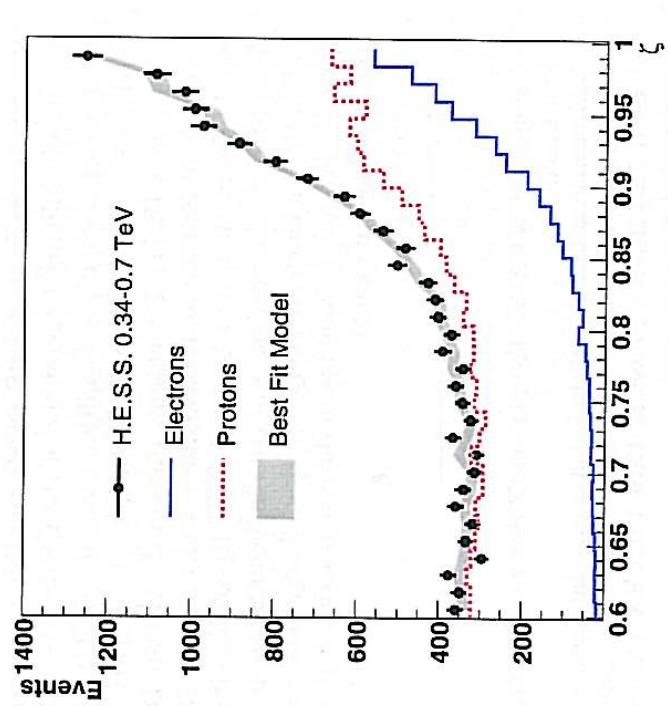

FIG. 1: The measured distribution of the parameter ζ, compared with distributions for simulated protons and electrons, for showers with reconstructed energy between 0.34 and 0.7 TeV (the energy range of the extension towards lower energies compared to the analysis presented in [8]). The best fit model combination of electrons and protons is shown as a shaded band. The proton simulations use the SIBYLL hadronic interaction model. Distributions differ from the ones presented in Fig. 1 of [8] because of the energy dependence of the ζ parameter.

Literature:

- Particle Physics and Cosmic Rays
  Thomas Gaisser
  Cambridge Univ. Press (UK, 1990)

- Production and propagation of cosmic ray positrons and electrons
  I.V. Moskalenko, A.W. Strong
  `arXiv:astro-ph/9710124`

- Positron propagation and fluxes from neutralino annihilation in the halo.
  Baltz, Joakim Edsjo
  `arXiv:astro-ph/9808243`

- PAMELA: A Payload for Antimatter Matter Exploration and Light-nuclei Astrophysics.
  PAMELA collaboration
  `arXiv:astro-ph/0608697`

- A new measurement of the antiproton-to-proton flux ratio up to 100 GeV in the cosmic radiation
  PAMELA collaboration
  `arXiv:0810.4994`

- An anomalous positron abundance in cosmic rays with energies 1.5.100 GeV.
  PAMELA collaboration
  `arXiv:0810.4995`

- Cosmic Rays At Earth
  Grieder
  Elsevier Science 2001

- Measurements of cosmic ray low-energy anti-proton and proton spectra in a transient period of the solar field reversal
  BESS collaboration
  `arXiv:astro-ph/0109007`

- An excess of cosmic ray electrons at energies of 300.800 GeV.
  ATIC collaboration
  Nature 456:362-365,2008

- Measurement of the Cosmic Ray e+ plus e- spectrum from 20 GeV to 1 TeV with the Fermi Large Area Telescope.
  FERMI collaboration
  `arXiv:0905.0025`

- The energy spectrum of cosmic-ray electrons at TeV energies
  HESS collaboration
  `arXiv:0811.3894`

- Probing the ATIC peak in the cosmic-ray electron spectrum with H.E.S.S.
  HESS collaboration
  `arXiv:0905.0105`